Molecular Vision 2025; 31:502-513 <http://www.molvis.org/molvis/v31/502>
Received 1 July 2025 | Accepted 10 December 2025 | Published 12 December 2025

Deciphering the genetic basis of inherited retinal dystrophies via whole-exome sequencing in a Turkish cohort

Zulal Keles,[1] Ozlem Ural Fatihoglu,[2] Ziya Ayhan,[2] Ali O. Saatci,[2] Ahmet O. Caglayan,[1] Ayfer Ulgenalp[1]

(Last two authors contributed equally to this work.)

[1]Department of Medical Genetics, Dokuz Eylül University, Izmir, Turkey; [2]Department of Ophthalmology, Dokuz Eylül University, Izmir, Turkey

Purpose: Inherited retinal dystrophies (IRDs) encompass a genetically and clinically heterogeneous group of disorders, with over 300 genes currently implicated. Early and precise genetic diagnosis is critical for advancing targeted gene therapies and personalized treatment strategies. This study aims to investigate genetic findings in IRDs using whole-exome sequencing (WES) in a cohort of affected individuals.
Methods: WES was performed on 34 unrelated probands diagnosed with diverse IRD subtypes. Variant analysis focused on identifying clinically relevant variants consistent with the patients' phenotypes and inheritance patterns, emphasizing novel and rare variants.
Results: Clinically relevant variants consistent with the patients' phenotypes and inheritance patterns were identified in 24 cases. Among these, four variants were novel: *RP2* c.181_182del, *CYP4V2* c.377T>G, *RPGR* c.1414G>A, and *RPE65* c.267C>G. Additionally, we identified a patient with isolated IRD carrying a homozygous *IFT81* c.1969C>T (p.Gln657Ter) variant, a gene typically associated with syndromic phenotypes. Furthermore, we reported a relatively rare presentation of ARSG-related Usher syndrome in a patient harboring a homozygous *ARSG* c.263G>T (p.Arg88Leu) alteration.
Conclusions: This study underscores the diagnostic power of WES in IRDs, revealing novel variants and supporting its integration into clinical practice to enhance early diagnosis and enable precision medicine.

Inherited retinal dystrophies (IRDs) are a clinically and genetically diverse group of disorders defined by abnormal function or degeneration of retinal pigment epithelial cells or photoreceptors [1], with reported prevalence estimates ranging from approximately 1 in 500 (0.2%) to 1 in 1,430 individuals in population-based studies [2-5]. Classification is often based on the type of photoreceptor predominantly affected (rod, cone, or rod-cone), the anatomic region involved (diffuse, macular, chorioretinal, or inner retinal/vitreoretinal), the presence of systemic involvement (syndromic versus isolated), or congenital/stationary forms [6,7]. IRDs are highly genetically heterogeneous, with autosomal recessive (AR), autosomal dominant (AD), X-linked, mitochondrial, and digenic inheritance patterns reported [1]. To date, more than 300 genes associated with IRDs have been identified in the Retinal Information Network database (RetNet). Over 80 syndromes have been reported in which IRDs are accompanied by involvement in other organs or systems. Most of these syndromes have AR inheritance and are included in two basic disease groups: ciliopathies and metabolic diseases of the newborn [8].

Correspondence to: Zulal Keles, Department of Medical Genetics, Dokuz Eylül University Mithatpasa Street, Inciraltı-Balcova, Izmir, Turkey, 35340; email: zulal.keles.93@gmail.com

By modern genetic techniques, the molecular diagnosis rate in IRDs ranges from 44% to 71% [9,10]. Understanding the genetic etiology enables the refinement of emerging treatment modalities, including gene therapies [6]. Retinal dystrophies are particularly well suited for gene replacement therapies due to their predominantly monogenic inheritance, the availability of vectors such as adeno-associated virus with high tropism for retinal cells, the relative ease of therapeutic application, and the immune-privileged status of retinal tissue [11]. The US Food and Drug Administration approved adeno-associated virus–based voretigene neparvovec-rzyl (Luxturna) for patients with Leber congenital amaurosis and early-onset retinitis pigmentosa who have biallelic variants in the *RPE65* gene. Gene therapy studies are continued for different genes [12].

In recent years, cohort studies on IRDs in Turkey have expanded significantly, driven by the widespread adoption of next-generation sequencing methods [13-16]. In our study, whole-exome sequencing (WES) was performed on 34 unrelated patients with various subtypes of IRDs. The primary objectives were to assess the diagnostic utility of WES in this patient cohort, characterize clinical subtypes, and analyze inheritance patterns, as well as gene and variant distributions.

METHODS

The research is a retrospective descriptive study conducted at Dokuz Eylul University Faculty of Medicine, Departments of Medical Genetics and Ophthalmology. The study protocol was designed in accordance with the principles of the Declaration of Helsinki, and ethics committee approval was obtained under decision number 2022/18–01 of the Non-Invasive Research Ethics Committee of Dokuz Eylül University. Patients who underwent WES with a preliminary diagnosis of IRD between December 2019 and June 2021 were included in the study. Written informed consent was obtained from all participants (or their legal guardians for underage patients) enrolled in the study. The age, gender, initial and current symptoms, age at disease onset, ophthalmologic and dysmorphologic examinations results, disease progression, and, when available, findings from fundus autofluorescence, optical coherence tomography (OCT), and electroretinography (ERG) records (ERG was available for only two patients [P15, P31], who had the test performed at another center), current treatments, family history, and genetic test results of the participants were evaluated.

DNA extraction: A total of 4 ml of peripheral blood samples was collected in EDTA tubes for molecular studies at Dokuz Eylul University Genetic Diseases Evaluation Center. To obtain purified total genomic DNA, DNA was isolated from 200 µl of blood from each patient using the spin-column DNA isolation technique with the QIAamp DNA Blood Mini kit (Qiagen, Hilden, Germany) and the Qiacube automated DNA isolation device (Qiagen), according to the manufacturer's instructions. The NanoDrop ND1000 Spectrophotometer device (Thermo Fisher Scientific, Waltham, MA) was used to measure the concentration and purity of the isolated DNA samples.

Whole-exome sequencing: The Twist Human Comprehensive Exome kit (Twist Bioscience, San Francisco, CA) was employed in accordance with the manufacturer's recommendations for WES, using DNA samples with a purity (A260/A280 ratio) of 1.8 to 2.0 and a concentration of at least 40 ng/µl. FASTQ format data obtained from WES were aligned to the reference genome (GRCh37/hg19) and processed through several steps, including sequencing, variant calling, reliability scoring, and variant annotation. The SEQ (Genomize, Istanbul, Turkey) analysis platform was used during these stages. For alignment and sequencing, the Burrows-Wheeler Aligner program was used, while variant calling was performed using the optimized haplotype-based FreeBayes program. Reliability assessments of variants were based on primary and secondary coverage thresholds, alternative/allele ratio thresholds, strand bias value thresholds, and alternative/allele ratio parameters in both strands for heterozygous variants. Variants classified as unreliable were excluded from further analysis. Following these bioinformatic processes, the data were converted to variant call format (VCF).

Prioritization of genetic variants: The pathogenicity of variants was assessed using guidelines from the American College of Medical Genetics and Genomics, published in 2015 [17], and the Association for Clinical Genomic Science, published in 2024. Variants were classified into five categories: benign, likely benign, uncertain clinical significance, likely pathogenic, and pathogenic. Variants with a read depth of <10× were excluded from the analysis. Variants with a minor allele frequency of <5% in both the in-house database and population databases, including the 1000 Genomes Project, exome aggregation consortium (ExAC), genome aggregation database (gnomAD), and single-nucleotide polymorphism database (dbSNP), which were within exons and/or flanking intronic regions, were prioritized to identify potentially disease-associated variants and to avoid missing hypomorphic alleles. Clinical interpretation of the relevant genes was performed using the Online Mendelian Inheritance in Man (OMIM) and Retinal Information Network databases. Additionally, Human Phenotype Ontology terms corresponding to the patients' clinical features were applied in the analysis. The ClinVar and Leiden Open Variation Database resources were also consulted in the classification of variants.

Novel variants have been submitted to ClinVar. The accession numbers for novel variants are SCV006079509, SCV006082497, SCV006082503, SCV006082511, SCV006082518, and SCV006082520.

Sanger sequencing: The candidate variants identified in 17 patients were confirmed by Sanger sequencing (Appendix 1). Validation was planned for the remaining patients. Primers were designed using NCBI Primer Design. The obtained sequence data were analyzed using the CLC Genomics Workbench (Qiagen) program. Segregation analysis was conducted contingent upon the availability of DNA samples from relatives.

RESULTS

Clinical presentations: A total of 34 patients, with a mean age of 36 years (range: 8–71), were enrolled in this study. Among the various IRD subtypes diagnosed (Figure 1), retinitis pigmentosa (RP) was the most prevalent. The average age of symptom onset was 16 years (range: 0–42), with four patients exhibiting symptoms during infancy. Best-corrected visual acuity varied widely, ranging from light perception (p+) to 1.0. The diagnoses and ophthalmic evaluations are summarized in Appendix 2. Representative fundus autofluorescence

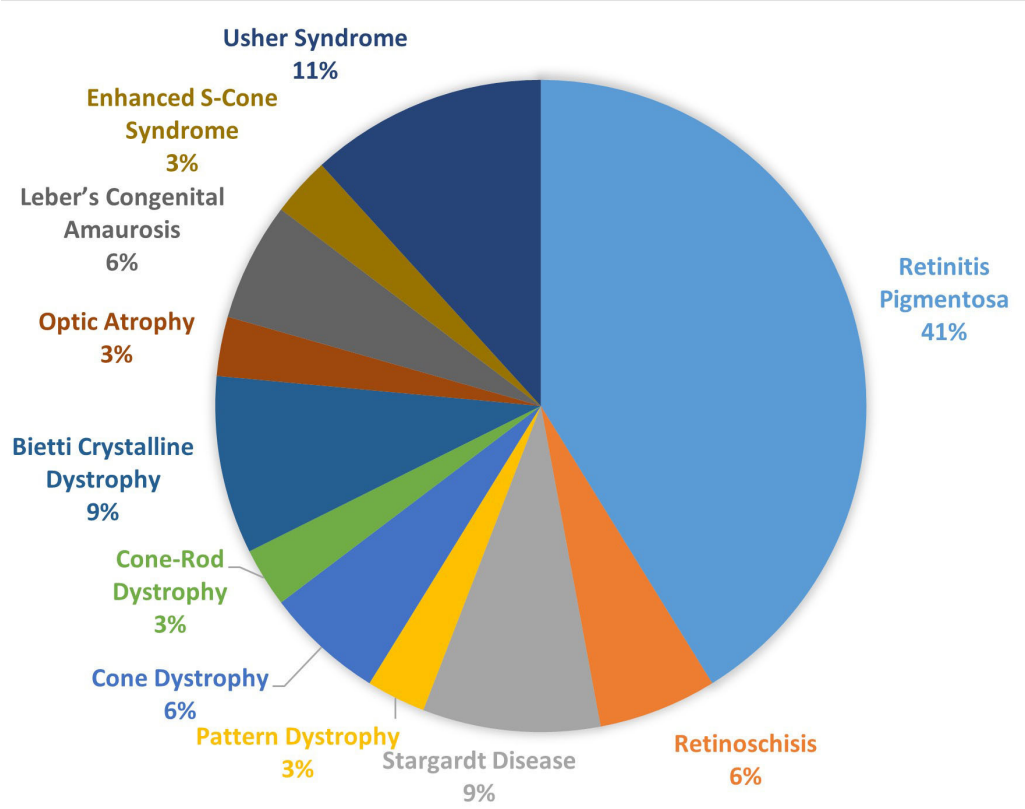

Figure 1. Distribution of disease subgroups among the study cohort. The pie chart illustrates the proportion of patients in each disease subgroup, expressed as percentages of the total cohort (n = 34). Subgroups were defined according to clinical presentation and molecular findings.

and OCT images from six patients are shown in Figure 1, Figure 2, and Figure 3.

Among the 34 patients diagnosed, 5 had syndromic IRD. In patient (P) 2 and P4, initially diagnosed with Usher syndrome, hearing impairment emerged in childhood,

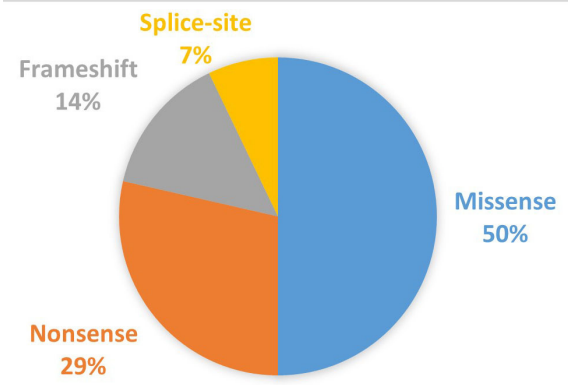

Figure 2. Distribution of potential disease-causing variants (DCVs) among solved/potentially solved patients. Potential DCVs were identified in 24 of the 34 patients, consistent with their clinical phenotypes and inheritance patterns. The figure illustrates the distribution of variant types (missense, nonsense, splice site, and frameshift). For individuals with dual molecular diagnoses, each variant was considered separately, resulting in a total of 28 distinct variants included in the analysis. Variants listed in Appendix 9 are represented here. For P1, three variants (a complex variant in *ABCA4* and an additional variant in *CLRN1*) were evaluated individually.

followed by visual symptoms at ages 12 and 17, respectively. Neither exhibited vestibular dysfunction, suggesting Usher syndrome type II as the most likely diagnosis. P4, who experienced visual symptoms at age 7, required a cochlear implant due to bilateral congenital hearing loss (HL) and exhibited vestibular dysfunction, consistent with Usher syndrome type I. In P26, hearing loss began in childhood, while visual symptoms appeared at age 37, raising suspicion of atypical Usher syndrome. P30 presented with epilepsy at age 7, progressive cognitive decline, and nyctalopia beginning at age 14. Fundus examination revealed retinitis punctata albescens with macular involvement, suggesting a syndromic form of RP.

In this cohort, 20 (59%) had parents who were second-degree cousins or closer, while 7 patients had parents from the same village. Pedigrees of patients carrying potential disease-causing variants are shown in Appendix 1, Appendix 3, Appendix 4, Appendix 5, Appendix 6 and Appendix 7. Four patients without reported consanguinity (P18, P20, P21, P22) carried homozygous variants, as illustrated in their pedigrees (Appendix 5, Appendix 6), suggesting possible cryptic relatedness.

Genetic findings: WES achieved an average coverage of 95× across the entire capture region, with more than 90% of the targeted bases covered by at least 20 reads (Appendix 8). Potential disease-causing variants (DCVs) were identified in 24 of the 34 patients, aligning with their clinical phenotypes and inheritance patterns. The affected genes included *ABCA4* (5), *CYP4V2* (3), *RS1* (2), *RPE65* (2), *CLRN1*, *USH2A*, *USH1C*, *RPGRIP1*, *RP2*, *BEST1*, *PCARE*, *OPA1*, *IMPG1*, *DRAM2*, *NR2E3*, *IFT81*, *KCNV2*, *ARSG*, *MFSD8*, and *RPGR* (Appendix 9). Among these, the homozygous *ABCA4* c.4640delA (p.Lys1547ArgfsTer34) variant was detected in two siblings (P22 with Stargardt's disease and P35 with IRD); however, to avoid data duplication, only one sibling was included in the study. All other variants were unique to individual patients.

According to guidelines from the American College of Medical Genetics and Genomics and the Association for Clinical Genomic Science, the 28 identified variants in 24 patients were classified as 22 likely pathogenic (LP) and 6 variants of uncertain significance (VUS). Of the variants considered causative, 20 were homozygous (71%), 4 were hemizygous, and 4 were heterozygous. In total, 50% of the identified variants were missense (Figure 2).

One patient (P1) carried a biallelic complex variant in *ABCA4*. P1 presented with symptom onset at age 11, best-corrected visual acuity of 0.1/0.1 at age 23, and retinal atrophy with flecks (Figure 3A). Additionally, P1 carried a heterozygous *CLRN1* c.93del (p.Leu32CysfsTer4) frameshift variant, predicted to result in a premature stop codon. *CLRN1*

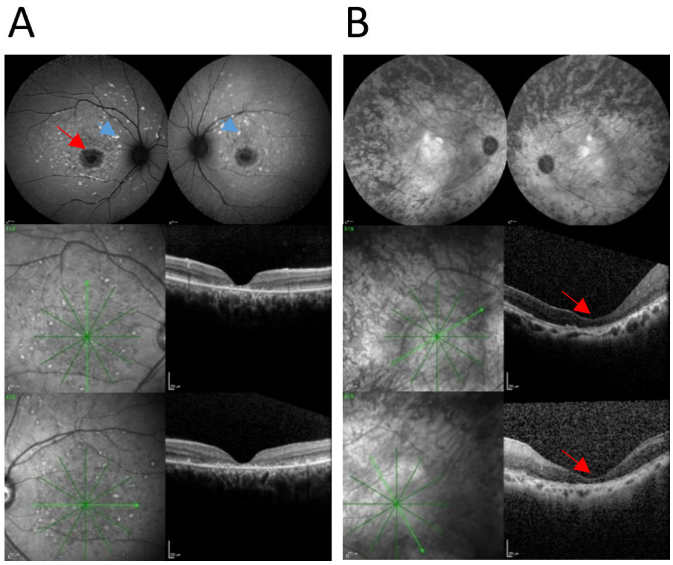

Figure 3. Fundus autofluorescence (FAF) and optical coherence tomography (OCT) of both eyes for P1 and P11. **A**. FAF images from P1 show a hyperautofluorescent parafoveal ring and scattered peripheral flecks of increased autofluorescence (blue arrowheads), along with central hypoautofluorescent lesions compatible with macular atrophy (red arrow). Corresponding OCT scans demonstrate preserved foveal architecture with subtle disruption in the outer retinal layers. B. FAF images from P11 with retinitis pigmentosa display widespread retinal atrophy. OCT scans reveal significant degeneration of the outer retina, including loss of the ellipsoid zone, which reveals macular atrophy (red arrows), and marked peripheral chorioretinal degeneration.

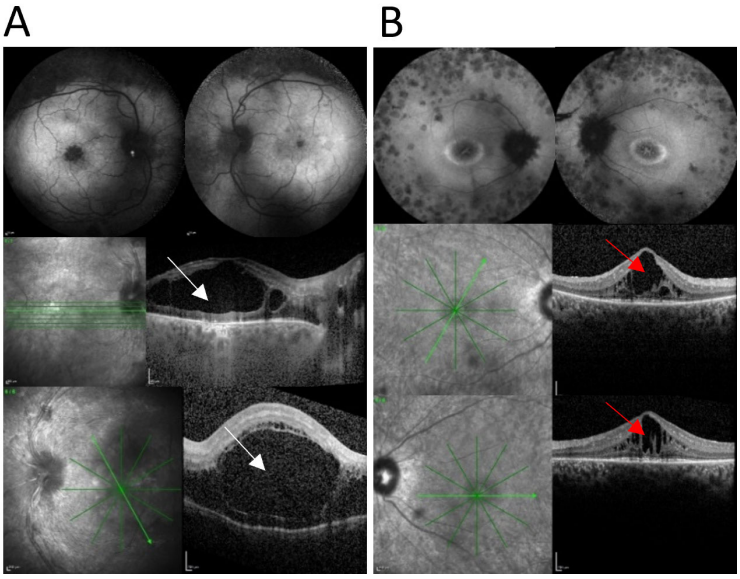

Figure 4. Fundus autofluorescence (FAF) and optical coherence tomography (OCT) of both eyes for P29 and P7. **A**. Images of P29 demonstrate peripheral hypoautofluorescence extending beyond the vascular arcades and a hyperautofluorescent ring at the transition zone on FAF. OCT images reveal foveal schisis (white arrows), consistent with concentric peripheral retinal degeneration characteristic of enhanced S-cone syndrome. **B**. P7 shows bilateral retinitis pigmentosa with widespread FAF abnormalities and cystoid macular edema on OCT (red arrows), indicating intraretinal fluid accumulation and advanced retinal dysfunction.

is associated with RP and AR Usher syndrome type IIIA (USH3: MIM 276,902). No additional pathogenic variants in *CLRN1* were detected, and P1 exhibited no RP, asymmetry between the eyes, or hearing loss.

Additionally, two patients had dual genetic diagnoses (P11, P19). P11 presented with progressive nyctalopia and blurred vision beginning at age 20, along with peripheral visual field defects. By age 48, his visual acuity had deteriorated to "counting fingers" at 2 m, and he underwent cataract surgery in both eyes. Fundus examination confirmed a diagnosis of RP (Figure 3B). Genetic analysis revealed a hemizygous c.181_182del (p.Gln61ValfsTer7) variant in *RP2*, which is associated with X-linked RP. Additionally, the patient was found to carry a heterozygous LP c.425G>A (p.Ser142Asn) variant in *BEST1*, which has been linked to vitelliform macular dystrophy (VMD2: OMIM 153700). However, given the clinical findings, the c.181_182del variant in *RP2* was considered dominant in this patient's phenotype.

In P19, a heterozygous c.1348G>A (p.Val450Met) variant in *OPA1* related to AD optic atrophy (OPA1: OMIM 165500) was identified, along with a heterozygous c.1711C>T (p.Arg571Ter) variant in *IMPG1*, which is associated with AD, AR vitelliform macular dystrophy, and AD RP. Fundus examination revealed optic disc pallor and cupping, suggesting that the *OPA1* variant predominantly influences the patient's phenotype.

In two patients, the diagnosis changed following genetic evaluation: P10 from rod-cone dystrophy to Leber congenital amaurosis and P21 from Stargardt's disease to cone-rod dystrophy. In one patient (P29), the diagnosis was clarified to enhanced S-cone syndrome (Figure 4A) following genetic testing.

Five of 34 patients (P7, P17, P23, P26, P30) carried candidate variants classified as VUS that may contribute to their clinical symptoms. A homozygous c.1969C>T (p.Gln657Ter) variant was identified in *IFT81* in P7, who was diagnosed with RP (Figure 4B). The variant is in exon 19, the final exon, and introduces a premature stop codon, truncating the protein by 20 amino acids. However, the protein is predicted to evade nonsense-mediated messenger RNA decay. The variant is present in the longest and most highly expressed transcript in the retina and is absent in population and in-house databases (PVS1_Moderate, PM2). Sanger sequencing confirmed the variant as homozygous in P7, heterozygous in the healthy mother, and absent in the healthy sister.

In P17, who was evaluated with a preliminary diagnosis of Bietti crystalline dystrophy (Figure 5B), a homozygous c.377T>G (p.Phe126Cys) variant in *CYP4V2* was detected. AlphaMissense score of the variant is 0.65.

P23, evaluated for RP, had a family history suggestive of X-linked inheritance. A hemizygous c.1414G>A (p.Asp472Asn) variant in exon 11 of *RPGR*, which is

associated with X-linked IRD, was identified. According to the SpliceAI prediction program, this variant may affect splicing, with a score of 0.82.

In P26, a homozygous c.263G>T (p.Arg88Leu) variant was identified in *ARSG*, which is associated with Usher syndrome type IV in the OMIM database. The variant is rare (<0.01% frequency in population databases) and has not been previously reported in the literature (PM2). This variant is located in an evolutionarily conserved region across species and is predicted to be LP by AlphaMissense (0.9; PP3).

A homozygous *MFSD8* c.929G>A (p.Gly310Asp) variant was identified in P30, whereas both parents were heterozygous and exhibited no visual symptoms. This variant has been classified as LP in ClinVar, and its AlphaMissense score is 0.84.

Excluding the 24 patients with identified causative variants, LP variants were detected in a single allele in four patients (P5, P8, P25, and P34; Appendix 10). In P8, in addition to the common disease-causing variant *USH2A* c.2299delG (p.Glu767fs), a heterozygous *USH2A* c.682A>T (p.Asn228Tyr) variant was identified. However, segregation analysis revealed that both alterations were inherited paternally, ruling out a biallelic pathogenic effect. In P34, heterozygous LP variants were observed in *USP45* and *USH2A*; however, since both genes require biallelic variants to result in disease, a molecular basis for the phenotype could not be determined. The current understanding of digenic inheritance remains incomplete, and further studies are needed to establish its role in IRD pathogenesis.

In P14, no pathogenic, LP, or VUS were identified in *PRPH2*, *CTNNA1*, and *MAPKAPK3*, genes associated with pattern dystrophy. Given the presence of pervasive retinal drusen on OCT, basal laminar drusen was considered in the differential diagnosis, and a heterozygous *CFH* c.3607C>T (p.Arg1203Trp) variant was detected.

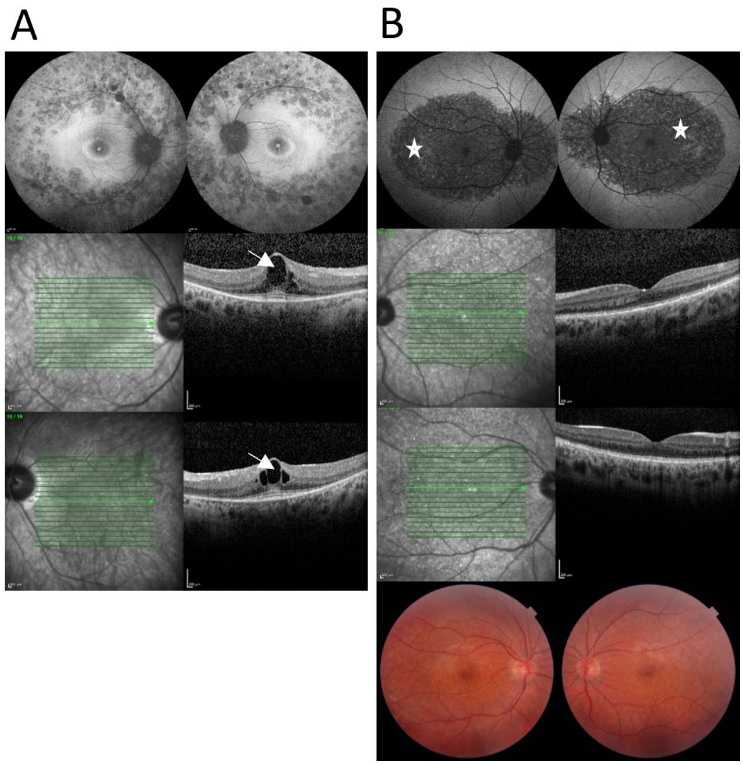

Figure 5. Fundus autofluorescence (FAF) and optical coherence tomography (OCT) of both eyes for P17 and P26, along with color fundus photography for P17. **A**. In P26, FAF images reveal a hyperautofluorescent ring surrounding the macular region, along with hypoautofluorescence at the level of the vascular arcades. The peripheral retina appears relatively preserved. OCT images confirm the presence of bilateral cystoid macular edema (indicated by white arrows) consistent with intraretinal fluid accumulation and retinal layer separation. **B**. In P17, FAF images show patchy areas of hypoautofluorescent areas, which correspond to retinal atrophy (denoted by white asterisks), as well as crystalline deposits scattered throughout the posterior pole. Color fundus photography corroborates these findings, showing relatively preserved macular pigmentation with visible crystalline material.

The six novel variants found in six patients had not been previously published in databases or in the literature (*CLRN1* c.93del, *RP2* c.181_182del, *CYP4V2* c.377T>G, *RPGR* c.1414G>A, *RPE65* c.267C>G, *USP45* c.931_932delAA; Appendix 11, Appendix 12, Appendix 13, Appendix 14, Appendix 15, and Appendix 16).

DISCUSSION

IRDs encompass a diverse group of diseases with a broad clinical and genetic spectrum [18]. In the literature, the most common IRD subtype across various populations is RP, with reported prevalence rates ranging from 32% to 48%, while syndromic cases account for 1% to 17% [3,9,10,16]. Similarly, in our study, RP was the most frequent diagnosis, affecting 41% of patients, and the proportions of isolated and syndromic patients (15%) aligned with the literature.

A genetic alteration consistent with the clinical phenotype was identified in 24 of 34 patients (71%) with retinal dystrophy who underwent WES. This diagnostic yield aligns with previous studies, which report WES detection rates ranging from 49% to 71% in IRDs [9,19,20].

Consanguinity rates in Turkey vary by source. According to the Turkish Statistical Institute's 2024 data, 8.1% of individuals in their most recent marriages married a first-degree cousin, whereas the Turkish Demographic and Health Survey 2018 reported a rate of 24%. Kaplan et al. [21] further noted that 18.5% of marriages were between second-degree cousins or closer. In our cohort, the reported consanguinity rate is 59%, but it is likely higher due to possible cryptic relatedness. Regional IRD studies also report high—but variable—consanguinity rates: a nationwide Israeli IRD series reported ~37% consanguineous families [22], a Jordanian cohort 71% [20], while Egyptian cohorts recorded 5.9% consanguinity, though data were missing for 58.3% of patients, highlighting limitations in reporting [23].

Given the high rate of consanguineous marriages in Turkey, AR inheritance was expected to predominate, which aligns with our finding of homozygous variants in 83% of patients. A WES study involving 28 patients conducted in Turkey found that 78% of the patients had a history of consanguineous marriage. The study revealed a wide distribution of genes and variants, with *MERTK* variants being the most prevalent [13]. Another Turkish study of 354 patients with IRDs using targeted gene panels reported a 58% diagnostic yield, with 87% of cases showing AR inheritance and *ABCA4* as the most frequently implicated gene, consistent with our findings [16]. Together, these observations emphasize that consanguinity is a major contributor to AR IRD in Turkey, although cross-study comparisons should account for differences in data availability and reporting practices.

The *ABCA4* gene is associated with Stargardt's disease (STGD1, OMIM 248200), RP, and cone-rod dystrophy. To date, over 1,500 DCVs in *ABCA4* have been reported, exhibiting a broad phenotypic spectrum from severe early-onset to milder late-onset forms. The residual activity of the ABCA4 protein influences disease severity, with null alleles typically causing more severe phenotypes [24]. In our cohort, four distinct homozygous *ABCA4* DCVs were identified in four patients, all presenting with childhood-onset symptoms (mean age: 10 years).

A homozygous complex variant (*ABCA4* c.4102C>T; c.5603A>T) was identified in P1, initially diagnosed with Stargardt's disease. The c.4102C>T variant has been previously reported in compound heterozygous cases of Stargardt's disease and generalized IRDs [25]. In silico functional analysis suggests that a Grantham score above 90 may correlate with early-onset disease, and c.4102C>T has a score of 180, supporting its pathogenicity [26]. The c.5603A>T variant, a hypomorphic allele with a minor allele frequency of 7%, is typically linked to late-onset disease with foveal sparing. However, when found in *cis* with another DCV, it may lead to early-onset and severe phenotypes [27]. This specific biallelic complex variant has not been previously reported in the literature. In addition, a heterozygous *CLRN1* c.93del (p.Leu32CysfsTer4) frameshift variant was identified in P1. Previous studies suggest that *CLRN1* may contribute to isolated RP [28,29], although its exact contribution remains uncertain.

Among the patients with VUS, P7, P26, and P30 were selected for detailed discussion due to their clinical presentations and the potential relevance of these variants, as supported by available literature. *IFT81*, located at 12q24.11 and consisting of 19 exons, is associated with short-rib thoracic dysplasia 19 with or without polydactyly (SRTD19: OMIM 617895). The gene encodes the 676-amino-acid intraflagellar transport 81 (IFT81) protein, which consists of four "coiled-coil" domains and an NCD80-NUF2 calponin homology (NN-CH) domain, with the tubulin-binding site at the N-terminal end playing a key role in ensuring cilia integrity. As part of the IFT-B core complex, IFT81 is responsible for anterograde transport [30]. The homozygous c.1969C>T (p.Gln657Ter) variant identified in *IFT81* in P7, reported in the literature in a patient with RP, mixed-type HL, and syndromic ciliopathy with skeletal abnormalities, was deemed pathogenic [31]. Conditions related to *IFT81* range from neonatal lethal asphyxiating thoracic dysplasia to isolated IRD [30-34] (Appendix 17). Similar to previously

reported cases [30], P7 had a history of delayed speech. However, unlike those cases, no additional systemic findings were present, and the diagnosis was determined to be isolated IRD. Based on these findings, the c.1969C>T variant is suggested to be responsible for P7's clinical presentation. However, further research is essential to confirm the diagnosis and establish the variant's impact on the phenotype.

The onset of RP in atypical Usher syndrome related to *ARSG*, as reported in the literature, ranges from 35 to 60 years [35-38], which aligns with P26's nyctalopia symptoms, which began at age 37. In line with prior studies, P26's vestibular system remained intact. Although HL in previously reported cases generally occurred after the age of 40, childhood and young adult HL have also been documented [37,39]. In P26, HL manifested in childhood. These findings suggest that the age at which HL develops in ARSG-related US may be variable or that HL may be underdiagnosed due to its slow progression. The literature also describes a characteristic pattern of retinal degeneration, which includes ring-shaped atrophy bordering the vascular arcade, bone-spicule pigmentation in the mid-periphery, and relative sparing of the distal periphery. These specific retinal features were observed in P26, who also exhibited bilateral cystoid macular edema (Figure 5A), similar to the findings reported by Fowler et al. [35]. Previous reports have described disease-associated missense variants near the variant we identified [36,39].

The *MFSD8* homozygous c.929G>A (p.Gly310Asp) variant identified in P30 has been previously documented in patients with variant late infantile neuronal ceroid lipofuscinosis [40] and in cases of cone dystrophy [41].

Our study has several limitations that should be considered. In 10 of our patients with IRDs, no variants were identified that could clearly account for the observed phenotypes. This underscores the genetic complexity of IRDs and highlights the limitations of WES, which may fail to detect certain variants, such as deep intronic changes, alterations in the 5′ and 3′ UTRs, structural variants, or large deletions/insertions. It is also possible that yet unidentified genes associated with retinopathy may contribute to these probands. Additionally, some variants may remain uninterpretable because segregation analysis and functional studies were not performed. Another limitation is the relatively small sample size, which may have restricted the detection of frequently reported causal variants in the Turkish population. Most analyses were performed on index cases, and the cohort included patients spanning a wide range of disease subtypes and ages. Some patient records were incomplete or unavailable, which limited accurate subclassification of all IRD cases; this represents a limitation of our retrospective study. Sequential clinical assessments were not consistently available, and follow-up was limited. ERG data were available for only two patients due to a lack of ERG equipment in our center. The limited availability of ERG data represents a major constraint and may affect diagnostic accuracy.

Few studies have been conducted on retinal dystrophies in Turkey, and the approach to this group of diseases is evolving. This study presents a cross-sectional sample of patients with IRDs using WES in the Turkish population. In 19 of 34 patients with IRDs, LP variants were identified that were consistent with their clinical presentations. Additionally, potentially deleterious variants classified as VUS were detected in five patients. We discussed a patient with isolated IRD associated with the *IFT81*, which typically leads to a syndromic phenotype. The variants identified in six patients have not been previously reported, and we present these novel variants to the literature. The increase in case reports and functional studies in this disease group will facilitate a better understanding of molecular mechanisms and will lay the groundwork for accelerating gene therapy research.

APPENDIX 1. SUPPLEMENTARY FIGURE 1.

To access the data, click or select the words "Appendix 1." Pedigrees of patients carrying potential disease-causing variants (DCVs). Panels show: (a) P1, (b) P2, (c) P4, (d) P6. DCVs detected in probands are indicated below the individual using the following notation: M/M (homozygous), M/WT (heterozygous), M (hemizygous). Genotypes of family members included in the analysis are represented similarly. In each figure, 'M' denotes the specific variant identified in the proband. The corresponding variant is detailed in the upper-left corner of the figure. A double horizontal line between individuals indicates consanguinity, whereas a line consisting of one solid and one dashed segment represents a marriage between individuals from the same village.

APPENDIX 2. SUPPLEMENTARY TABLE 1.

To access the data, click or select the words "Appendix 2." Clinical findings of probands. Abbrevations: AF: autofluorescence, BCVA: Best corrected visual acuity, DVA: decreased visual acuity, ERG: electroretinography, F: female, FAF: fundus autofluorescence, FCM: finger counting from () meter, HL: hearing Loss, HM: hand motion, M: male, MR: mental retardation, NA: not available, OCT: optical coherence tomography, OCTA: optical coherence tomography angiography, p+p --: perception is present/projection is absent, SNHL: sensorineural hearing loss. a : The Snellen test was used

APPENDIX 3. SUPPLEMENTARY FIGURE 2.

To access the data, click or select the words "Appendix 3." Pedigrees of patients carrying potential disease-causing variants (DCVs). Panels show: (a) P7, (b) P9, (c) P10, (d) P11. DCVs detected in probands are indicated below the individual using the following notation: M/M (homozygous), M/WT (heterozygous), M (hemizygous). Genotypes of family members included in the analysis are represented similarly. In each figure, 'M' denotes the specific variant identified in the proband. The corresponding variant is detailed in the upper-left corner of the figure. A double horizontal line between individuals indicates consanguinity, whereas a line consisting of one solid and one dashed segment represents a marriage between individuals from the same village.

APPENDIX 4. SUPPLEMENTARY FIGURE 3.

To access the data, click or select the words "Appendix 4." Pedigrees of patients carrying potential disease-causing variants (DCVs). Panels show: (a) P12, (b) P13, (c) P14, (d) P17. DCVs detected in probands are indicated below the individual using the following notation: M/M (homozygous), M/WT (heterozygous), M (hemizygous). Genotypes of family members included in the analysis are represented similarly. In each figure, 'M' denotes the specific variant identified in the proband. The corresponding variant is detailed in the upper-left corner of the figure. A double horizontal line between individuals indicates consanguinity, whereas a line consisting of one solid and one dashed segment represents a marriage between individuals from the same village.

APPENDIX 5. SUPPLEMENTARY FIGURE 4.

To access the data, click or select the words "Appendix 5." Pedigrees of patients carrying potential disease-causing variants (DCVs). Panels show: (a) P18, (b) P19, (c) P20, (d) P21. DCVs detected in probands are indicated below the individual using the following notation: M/M (homozygous), M/WT (heterozygous), M (hemizygous). Genotypes of family members included in the analysis are represented similarly. In each figure, 'M' denotes the specific variant identified in the proband. The corresponding variant is detailed in the upper-left corner of the figure. A double horizontal line between individuals indicates consanguinity, whereas a line consisting of one solid and one dashed segment represents a marriage between individuals from the same village.

APPENDIX 6. SUPPLEMENTARY FIGURE 5.

To access the data, click or select the words "Appendix 6." Pedigrees of patients carrying potential disease-causing variants (DCVs). Panels show: (a) P22, (b) P23, (c) P24, (d) P26. DCVs detected in probands are indicated below the individual using the following notation: M/M (homozygous), M/WT (heterozygous), M (hemizygous). Genotypes of family members included in the analysis are represented similarly. In each figure, 'M' denotes the specific variant identified in the proband. The corresponding variant is detailed in the upper-left corner of the figure. A double horizontal line between individuals indicates consanguinity, whereas a line consisting of one solid and one dashed segment represents a marriage between individuals from the same village.

APPENDIX 7. SUPPLEMENTARY FIGURES 6.

To access the data, click or select the words "Appendix 7." Pedigrees of patients carrying potential disease-causing variants (DCVs).

APPENDIX 8. SUPPLEMENTARY TABLE 2.

To access the data, click or select the words "Appendix 8." Whole exome sequencing quality scores of probands.

APPENDIX 9. CAUSATIVE AND POTENTIALLY CAUSATIVE VARIANTS IN PATIENTS WITH INHERITED RETINAL DYSTROPHY.

To access the data, click or select the words "Appendix 9." This table presents genetic variant data for patients whose clinical diagnosis could be confirmed by genetic findings. The table contains patient ID, diagnosis, gene transcript, inheritance pattern, variant location (exon/intron), genomic locations, cDNA and protein changes, dbSNP ID (for previously reported variants) or ClinVar accession number (for variants submitted to ClinVar by the authors), zygosity, REVEL score, ClinVar annotation, ACMG classification, and relevant references. Variants include pathogenic, likely pathogenic, and variants of uncertain significance (VUS). *: ABCA4 variants in P1 are presented in cis, with annotations for each variant-including exon number, dbSNP ID, ClinVar, ACMG classification, and reference information-provided separately, using a semicolon. a:Genomic locations have been added based on GRCh37. Abbrevations: AD: autosomal dominant, AR: autosomal recessive, E: exon, Hem: hemizygous, Het: heterozygous, Hom: homozygous, IVS: intervening sequence, LP: likely pathogenic, P: pathogenic, VUS: variant of uncertain clinical significance, XL: X-linked, a: inheritance pattern not specified. For P1, P11, and P19, the

variant in the gene associated with the retinal dystrophy subtype consistent with the clinical diagnosis is designated as the 'disease-associated variant,' whereas the additional likely pathogenic variant identified in a gene linked to a different retinal dystrophy subtype is reported as an 'incidental finding' in the 'gene/transcript' column.

APPENDIX 10. SUPPLEMENTARY TABLE S3.

To access the data, click or select the words "Appendix 10." Variants identified in unsolved probands.

APPENDIX 11. SUPPLEMENTAL FIGURE 7.

To access the data, click or select the words "Appendix 11." IGV image of the homozygous novel CLRN1 c.93del (p.Leu32CysfsTer40) variant in P1, showing the aligned sequencing reads and the variant position.

APPENDIX 12. SUPPLEMENTAL FIGURE 8.

To access the data, click or select the words "Appendix 12." IGV image of the hemizygous novel RP2 c.181_182del (p.Gln61ValfsTer7) variant in P11, showing the aligned sequencing reads and the variant position.

APPENDIX 13. SUPPLEMENTAL FIGURE 9.

To access the data, click or select the words "Appendix 13." IGV image of the homozygous novel CYP4V2 c.377T>G (p.Phe126Cys) variant in P17, showing the aligned sequencing reads and the variant position.

APPENDIX 14. SUPPLEMENTAL FIGURE 10.

To access the data, click or select the words "Appendix 14." IGV image of the hemizygous novel RPGR c.1414G>A (p.Asp472Asn) variant in P23, showing the aligned sequencing reads and the variant position.

APPENDIX 15. SUPPLEMENTAL FIGURE 11.

To access the data, click or select the words "Appendix 15." IGV image of the homozygous novel RPE65 c.267C>G (p.Tyr89Ter) variant in P32, showing the aligned sequencing reads and the variant position.

APPENDIX 16. SUPPLEMENTAL FIGURE 12.

To access the data, click or select the words "Appendix 16." IGV image of the heterozygous novel USP45 c.931_932delAA (p.Lys311fs) variant in P34, showing the aligned sequencing reads and the variant position.

APPENDIX 17. SUPPLEMENTARY TABLE S4.

To access the data, click or select the words "Appendix 17." Clinical presentation of patients associated with IFT81 gene in literature.

ACKNOWLEDGMENTS

The study's authors would like to thank the probands and their families for their assistance in completing this study. Conflict of Interest: The authors declare no conflict of interest. Funding Information: No funding was received for this study from any organizations. Data Availability Statement: Anonymous data used in this article are available on request from the corresponding author. Author Contributions: Z.K., A.O.C., and A.U. contributed to the conception and design of the study. Z.K., O.U.F., Z.A., A.O.S., A.O.C., and A.U. to the clinical evaluation of the patients and sample collection. Z.K. and A.O.C. analyzed the WES data. Z.K., A.O.C., and A.U. performed Sanger confirmation. Z.K. wrote the manuscript, which was reviewed by all authors. A.O.C. and A.U. participated in the study supervision. The authors declare no conflict of interest. The authors declare that they have no known competing financial interests or personal relationships that could have appeared to influence the work reported in this paper.

REFERENCES

1. Ben-Yosef T. Inherited Retinal Diseases. Int J Mol Sci 2022; 23:13467-[PMID: 36362249].
2. Tawfik CA, Roshdy MM, Morris NM. Prevalence of inherited retinal diseases in a large Egyptian cohort. BMC Ophthalmol 2023; 23:422-[PMID: 37864132].
3. Lähteenoja L, Ohtonen P, Falck A, Rahikkala EJ. Characterisation and prevalence of inherited retinal diseases in the Finnish population reveals enrichment of population-specific phenotypes and causative variants. Br J Ophthalmol 2025; 109:852-7. [PMID: 40571344].
4. Shalom S, Ben-Yosef T, Sher I, Zag A, Rotenstreich Y, Poleg T, Birk OS, Gradstein L, Ehrenberg M, Deitch I, Mezer E, Hecht I, Pras E, Ramon D, Khateb S, Zur D, Newman H, Kharouba R, Goldenberg-Cohen N, Leibu R, Soudry S, Perlman I, Banin E, Sharon D. Nationwide Prevalence of Inherited Retinal Diseases in the Israeli Population. JAMA Ophthalmol 2024; 142:609-16. [PMID: 38753338].
5. Abbass NJ, Yazji I, Allan KC, Kaelber DC, Talcott KE, Singh RP. Trends and Disparities in the Incidence and Prevalence of Inherited Retinal Diseases in the United States. Am J Ophthalmol 2025; 279:165-73. [PMID: 40706695].
6. Henderson RH. Inherited retinal dystrophies. Paediatrics and Child Health (United Kingdom) 2020; 30:19-27. Internet.

7. Sabbaghi H, Madani S, Ahmadieh H, Daftarian N, Suri F, Khorrami F, Saviz P, Shahriari MH, Motevasseli T, Fekri S, Nourinia R, Moradian S, Sheikhtaheri A. A health terminological system for inherited retinal diseases: Content coverage evaluation and a proposed classification. PLoS One 2023; 18:e0281858[PMID: 37540684].

8. Tatour Y, Ben-Yosef T. Syndromic Inherited Retinal Diseases: Genetic, Clinical and Diagnostic Aspects. Diagnostics (Basel) 2020; 10:10-Internet[PMID: 33023209].

9. Riera M, Navarro R, Ruiz-Nogales S, Méndez P, Burés-Jelstrup A, Corcóstegui B, Pomares E. Whole exome sequencing using Ion Proton system enables reliable genetic diagnosis of inherited retinal dystrophies. Sci Rep 2017; 7:42078-[PMID: 28181551].

10. Kim MS, Joo K, Seong MW, Kim MJ, Park KH, Park SS, Woo SJ. Genetic mutation profiles in Korean patients with inherited retinal diseases. J Korean Med Sci 2019; 34:.

11. Chiu W, Lin TY, Chang YC, Isahwan-Ahmad Mulyadi Lai H, Lin SC, Ma C, Yarmishyn AA, Lin SC, Chang KJ, Chou YB, Hsu CC, Lin TC, Chen SJ, Chien Y, Yang YP, Hwang DK. An update on gene therapy for inherited retinal dystrophy: Experience in leber congenital amaurosis clinical trials. Int J Mol Sci 2021; 22:4534-[PMID: 33926102].

12. Brar AS, Parameswarappa DC, Takkar B, Narayanan R, Jalali S, Mandal S, Fujinami K, Padhy SK. Gene Therapy for Inherited Retinal Diseases: From Laboratory Bench to Patient Bedside and Beyond. Ophthalmol Ther 2024; 13:21-50. [PMID: 38113023].

13. Basdemirci M, Kocak Eker H. Whole-Exome Sequencing in Turkish Patients with Inherited Retinal Dystrophies Reveals Novel Variants in Ten Genes. Mol Syndromol 2024; 15:202-10. [PMID: 38841332].

14. Kocaaga A, Aköz İÖ, Demir NU, Paksoy B. Identification of novel variants in retinitis pigmentosa genes by whole-exome sequencing. Rev Assoc Med Bras (1992) 2023; 69:e20221073[PMID: 37222315].

15. Duzkale N, Arslan U. Investigation of genotype-phenotype relationship in Turkish patients with inherited retinal disease by next generation sequencing. Ophthalmic Genet 2021; 42:674-84. [PMID: 34315337].

16. Ozguc Caliskan B, Uslu K, Sinim Kahraman N, Erkilic K, Oner A, Dundar M. Beyond the phenotype: Exploring inherited retinal diseases with targeted next-generation sequencing in a Turkish cohort. Clin Genet 2024; 106:258-66. [PMID: 38576124].

17. Richards S, Aziz N, Bale S, Bick D, Das S, Gastier-Foster J, Grody WW, Hegde M, Lyon E, Spector E, Voelkerding K, Rehm HL. ACMG Laboratory Quality Assurance Committee. Standards and guidelines for the interpretation of sequence variants: a joint consensus recommendation of the American College of Medical Genetics and Genomics and the Association for Molecular Pathology. Genet Med 2015; 17:405-24. [PMID: 25741868].

18. Wang L, Zhang J, Chen N, Wang L, Zhang F, Ma Z, Li G, Yang L. Application of Whole Exome and Targeted Panel Sequencing in the Clinical Molecular Diagnosis of 319 Chinese Families with Inherited Retinal Dystrophy and Comparison Study. Genes (Basel) 2018; 9:360-[PMID: 30029497].

19. Beryozkin A, Shevah E, Kimchi A, Mizrahi-Meissonnier L, Khateb S, Ratnapriya R, Lazar CH, Blumenfeld A, Ben-Yosef T, Hemo Y, Pe'er J, Averbuch E, Sagi M, Boleda A, Gieser L, Zlotogorski A, Falik-Zaccai T, Alimi-Kasem O, Jacobson SG, Chowers I, Swaroop A, Banin E, Sharon D. Whole Exome Sequencing Reveals Mutations in Known Retinal Disease Genes in 33 out of 68 Israeli Families with Inherited Retinopathies. Nature Publishing Group.2015.

20. Azab B, Dardas Z, Aburizeg D, Al-Bdour M, Abu-Ameerh M, Saleh T, Barham R, Maswadi R, Ababneh NA, Alsalem M, Zouk H, Amr S, Awidi A. Unique variant spectrum in a jordanian cohort with inherited retinal dystrophies. Genes (Basel) 2021; 12:593-[PMID: 33921607].

21. Kaplan S, Pinar G, Kaplan B, Aslantekin F, Karabulut E, Ayar B, Dilmen U. THE PREVALENCE OF CONSANGUINEOUS MARRIAGES AND AFFECTING FACTORS IN TURKEY: A NATIONAL SURVEY. J Biosoc Sci 2016; 48:616-30. [PMID: 26892044].

22. Sharon D, Ben-Yosef T, Goldenberg-Cohen N, Pras E, Gradstein L, Soudry S, Mezer E, Zur D, Abbasi AH, Zeitz C, Cremers FPM, Khan MI, Levy J, Rotenstreich Y, Birk OS, Ehrenberg M, Leibu R, Newman H, Shomron N, Banin E, Perlman I. A nationwide genetic analysis of inherited retinal diseases in Israel as assessed by the Israeli inherited retinal disease consortium (IIRDC). Hum Mutat 2020; 41:140-9. [PMID: 31456290].

23. Tawfik CA, Roshdy MM, Morris NM. Prevalence of inherited retinal diseases in a large Egyptian cohort. BMC Ophthalmol 2023; 23:422-[PMID: 37864132].

24. Lee W, Zernant J, Su PY, Nagasaki T, Tsang SH, Allikmets R. A genotype-phenotype correlation matrix for ABCA4 disease based on long-term prognostic outcomes. JCI Insight 2022; 7:e156154[PMID: 34874912].

25. Duno M, Schwartz M, Larsen PL, Rosenberg T. Phenotypic and genetic spectrum of Danish patients with ABCA4-related retinopathy. Ophthalmic Genet 2012; 33:225-31. [PMID: 22229821].

26. Cornelis SS, Bax NM, Zernant J, Allikmets R, Fritsche LG, den Dunnen JT, Ajmal M, Hoyng CB, Cremers FPM. In Silico Functional Meta-Analysis of 5,962 ABCA4 Variants in 3,928 Retinal Dystrophy Cases. Hum Mutat 2017; 38:400-8. [PMID: 28044389].

27. Zernant J, Lee W, Collison FT, Fishman GA, Sergeev YV, Schuerch K, Sparrow JR, Tsang SH, Allikmets R. Frequent hypomorphic alleles account for a significant fraction of ABCA4 disease and distinguish it from age-related macular degeneration. J Med Genet 2017; 54:404-12. [PMID: 28446513].

28. Khan MI, Kersten FFJ, Azam M, Collin RWJ, Hussain A, Shah STA, Keunen JEE, Kremer H, Cremers FPM, Qamar R, den Hollander AI. CLRN1 mutations cause nonsyndromic

retinitis pigmentosa. Ophthalmology 2011; 118:1444-8. [PMID: 21310491].

29. Sim PY, Jeganathan VSE, Wright AF, Cackett P. Case Report: Unilateral retinitis pigmentosa occurring in an individual with a mutation in the CLRN1 gene. BMJ Case Rep 2018; .
30. Perrault I, Halbritter J, Porath JD, Gérard X, Braun DA, Gee HY, Fathy HM, Saunier S, Cormier-Daire V, Thomas S, Attié-Bitach T, Boddaert N, Taschner M, Schueler M, Lorentzen E, Lifton RP, Lawson JA, Garfa-Traore M, Otto EA, Bastin P, Caillaud C, Kaplan J, Rozet JM, Hildebrandt F. IFT81, encoding an IFT-B core protein, as a very rare cause of a ciliopathy phenotype. J Med Genet 2015; 52:657-65. [PMID: 26275418].
31. Perea-Romero I, Blanco-Kelly F, Sanchez-Navarro I, Lorda-Sanchez I, Tahsin-Swafiri S, Avila-Fernandez A, Martin-Merida I, Trujillo-Tiebas MJ, Lopez-Rodriguez R, Rodriguez de Alba M, Iancu IF, Romero R, Quinodoz M, Hakonarson H, Garcia-Sandova B, Minguez P, Corton M, Rivolta C, Ayuso C. NGS and phenotypic ontology-based approaches increase the diagnostic yield in syndromic retinal diseases. Hum Genet 2021; 140:1665-78. [PMID: 34448047].
32. Duran I, Taylor SP, Zhang W, Martin J, Forlenza KN, Spiro RP, Nickerson DA, Bamshad M, Cohn DH, Krakow D. Destabilization of the IFT-B cilia core complex due to mutations in IFT81 causes a Spectrum of Short-Rib Polydactyly Syndrome. Sci Rep 2016; 6:34232-[PMID: 27666822].
33. Ashraf T, Vaina C, Giri D, Burren CP, James M, Offiah AC, Overton T, Baptista J, Ellard S, Smithson SF. Expanding the phenotypic spectrum of IFT81: Associated ciliopathy syndrome. Am J Med Genet A 2020; 182:2403-8. 2022[PMID: 32783357].
34. Dharmat R, Liu W, Ge Z, Sun Z, Yang L, Li Y, Wang K, Thomas K, Sui R, Chen R. IFT81 as a candidate gene for nonsyndromic retinal degeneration. Invest Ophthalmol Vis Sci 2017; 58:2483-90. [PMID: 28460050].
35. Fowler NH, El-Rashedy MI, Chishti EA, Vander Kooi CW, Maldonado RS. Multimodal imaging and genetic findings in a case of ARSG-related atypical Usher syndrome. Ophthalmic Genet 2021; 42:338-43. [PMID: 33629623].
36. Peter VG, Quinodoz M, Sadio S, Held S, Rodrigues M, Soares M, Sousa AB, Coutinho Santos L, Damme M, Rivolta C. New clinical and molecular evidence linking mutations in ARSG to Usher syndrome type IV. Hum Mutat 2021; 42:261-71. [PMID: 33300174].
37. Abad-Morales V, Navarro R, Burés-Jelstrup A, Pomares E. Identification of a novel homozygous *ARSG* mutation as the second cause of Usher syndrome type 4. Am J Ophthalmol Case Rep 2020; 19:100736[PMID: 32455177].
38. Khateb S, Kowalewski B, Bedoni N, Damme M, Pollack N, Saada A, Obolensky A, Ben-Yosef T, Gross M, Dierks T, Banin E, Rivolta C, Sharon D. A homozygous founder missense variant in arylsulfatase G abolishes its enzymatic activity causing atypical Usher syndrome in humans. Genet Med 2018; 20:1004-12. [PMID: 29300381].
39. Velde HM, Reurink J, Held S, Li CHZ, Yzer S, Oostrik J, Weeda J, Haer-Wigman L, Yntema HG, Roosing S, Pauleikhoff L, Lange C, Whelan L, Dockery A, Zhu J, Keegan DJ, Farrar GJ, Kremer H, Lanting CP, Damme M, Pennings RJE. Usher syndrome type IV: clinically and molecularly confirmed by novel ARSG variants. Hum Genet 2022; 141:1723-38. [PMID: 35226187].
40. Topçu M, Tan H, Yalnizoğlu D, Usubütün A, Saatçi I, Aynaci M, Anlar B, Topaloğlu H, Turanli G, Köse G, Aysun S. Evaluation of 36 patients from Turkey with neuronal ceroid lipofuscinosis: clinical, neurophysiological, neuroradiological and histopathologic studies. Turk J Pediatr 2004; 46:1-10. [PMID: 15074367].
41. Poncet AF, Grunewald O, Vaclavik V, Meunier I, Drumare I, Pelletier V, Bocquet B, Todorova MG, Le Moing AG, Devos A, Schorderet DF, Jobic F, Defoort-Dhellemmes S, Dollfus H, Smirnov VM, Dhaenens CM. Contribution of Whole-Genome Sequencing and Transcript Analysis to Decipher Retinal Diseases Associated with *MFSD8* Variants. Int J Mol Sci 2022; 23:4294-[PMID: 35457110].